A computational study of the aerodynamic performance of a dragonfly wing section in gliding flight

Bioinsp. Biomim. **3** (2008) 026004 (13pp) doi:10.1088/1748-3182/3/2/026004

A computational study of the aerodynamic performance of a dragonfly wing section in gliding flight

Abel Vargas, Rajat Mittal and Haibo Dong

Department of Mechanical and Aerospace Engineering, The George Washington University, Washington DC 20052, USA

E-mail: mittal@gwu.edu

Received 6 December 2007
Accepted for publication 2 May 2008
Published 23 May 2008
Online at stacks.iop.org/BB/3/026004

Abstract

A comprehensive computational fluid-dynamics-based study of a pleated wing section based on the wing of *Aeshna cyanea* has been performed at ultra-low Reynolds numbers corresponding to the gliding flight of these dragonflies. In addition to the pleated wing, simulations have also been carried out for its smoothed counterpart (called the 'profiled' airfoil) and a flat plate in order to better understand the aerodynamic performance of the pleated wing. The simulations employ a sharp interface Cartesian-grid-based immersed boundary method, and a detailed critical assessment of the computed results was performed giving a high measure of confidence in the fidelity of the current simulations. The simulations demonstrate that the pleated airfoil produces comparable and at times higher lift than the profiled airfoil, with a drag comparable to that of its profiled counterpart. The higher lift and moderate drag associated with the pleated airfoil lead to an aerodynamic performance that is at least equivalent to and sometimes better than the profiled airfoil. The primary cause for the reduction in the overall drag of the pleated airfoil is the negative shear drag produced by the recirculation zones which form within the pleats. The current numerical simulations therefore clearly demonstrate that the pleated wing is an ingenious design of nature, which at times surpasses the aerodynamic performance of a more conventional smooth airfoil as well as that of a flat plate. For this reason, the pleated airfoil is an excellent candidate for a fixed wing micro-aerial vehicle design.

(Some figures in this article are in colour only in the electronic version)

1. Introduction

The main source of lift and propulsion produced by insects is through the flapping of their wings. The dragonfly, considered a high performance flyer, is no exception. It has a flapping frequency between 30 Hz and 50 Hz (Rüppell 1989), and typically flies with its forewings and hindwings beating out of phase (Alexander 1984). Flapping flight of dragonflies has been studied extensively by Savage *et al* (1979), Alexander (1984), Azuma *et al* (1985), Somps and Luttges (1985), Rüppell (1989), Azuma (1992), Wakeling and Ellington (1997b), Azuma and Watanabe (1988) and Thomas *et al* (2004). However, gliding flight is also observed frequently in dragonflies; for instance, *Pantala flavescens* can sustain glides of 10–15 s at a flight speed of about 15 m s^{-1} (Hankin 1921). The dragonfly of the genus *Aeschna* is capable of gliding for up to 30 s without any appreciable loss in altitude (Brodsky 1994). Smaller dragonflies as those filmed in the experiments of Wakeling and Ellington (1997a) had gliding periods lasting 0.5 s, covering a distance of approximately 1 m, and achieving maximum gliding speeds of up to 2.6 m s^{-1}. The typical Reynolds number of dragonflies can range from 100 to 10 000 (Wakeling and Ellington 1997a), which can be categorized as being in the ultra-low Reynolds number flow regime.

Figure 1. An illustration of typical pleated cross-sections found in dragonfly wings (Kesel 2000).

Gliding flight is an advantageous flight mode as it requires virtually no effort from the dragonfly (Nachtigall 1974, May 1976, 1978). It is therefore not surprising that wing beat frequency declines considerably while the time spent gliding increases as the ambient temperature increases (Hankin 1921, May 1978, 1995). At high temperatures, large dragonflies run the risk of overheating during active flapping flight, and can avoid this by sustaining longer glides per wing beat (Miller 1987). It has also been hypothesized that dragonflies adopt this gliding mode to take advantage of convective cooling during hot weather.

In gliding flight, the dragonfly elevates into the air using powered (flapping) flight and makes use of potential energy to move horizontally above the ground (Brodsky 1994). It is well known that high aspect ratio wings are advantageous in gliding flight and this is the reason why wings with high aspect ratios are employed in sail planes as well as by large soaring birds. Interestingly, dragonflies have some of the highest aspect ratio wings in the insect world which allow them to possess a better glide performance and consume less energy during gliding (Ennos 1989). For particular *Aeschna juncea,* Ellington (1984b) calculated aspect ratios of 11.63 and 8.4 for the forewing and hindwing respectively. The crane fly (*Tipula paludosa*) is comparable to the dragonfly with an aspect ratio of about 11. The dragonfly's wing aspect ratio is quite high compared to other insects such as the fruit fly (*Drosophila virilis*) which has an aspect ratio of 2 (Vogel 1957) and the bumblebee (*Bombus terrestris*) with an aspect ratio of 6.4 (Ellington 1984b). The high aspect ratio dragonfly wings, which are narrow at the base with a greater wing area concentrated away from the base where airflow is the fastest, are features which probably also provide an aerodynamic advantage (Wootton and Kukalová-Peck 2000).

Dragonflies have highly corrugated wings where the pleated configuration varies along the spanwise and chordwise directions. The pleats provide stiffening against spanwise bending, while allowing for torsion and the development of camber (Hertel 1966, Newman *et al* 1977, Newman and Wootton 1986, Sudo and Tsuyuki 2000). Stiffness in the spanwise direction arises from the construction of a pleated wing since the longitudinal veins are located at the maximum and minimum peaks and are connected by the cross veins (Wootton 1981, 1990, 1991, 1992). The pleated wing is structurally stabilized primarily by the folded configurations, which increases flexural rigidity (Rees 1975a). Rigidity varies throughout the wing, and the factors which cause this variation are the depth of the pleats and the rigidity of the longitudinal cross veins (Wootton 1991).

The pleated structure found in dragonflies as seen in figure 1 does not resemble a typical engineered airfoil. Thus, it seems at the outset that such a pleated wing would have a poor aerodynamic performance (low lift, extremely high drag) due to its irregular shape. Steady flow experiments replicating gliding flight conducted on pleated models inspired by dragonflies (Rees 1975b, Rudolph 1977, Newman *et al* 1977, Buckholz 1986, Kesel 2000), real dragonfly wings (Okamoto *et al* 1996) and whole organism dragonflies in gliding flight (Wakeling and Ellington 1997a) have led to surprising and sometimes inconsistent conclusions, and these are discussed below.

Early wind tunnel experiments on scale-pleated models of insect wings conducted by Rees (1975b), Newman *et al* (1977) and Rudolph (1977) suggested that the pleated configuration has no aerodynamic significance. Rees (1975b) and Rudolph (1977) both concluded that fluid flowing over the pleated airfoil becomes trapped between the folds where it either becomes stagnant or rotates slowly, resulting in the pleated airfoil functioning as a streamlined airfoil. The only advantage of the pleated airfoil over the technical airfoils as noted by Rudolph (1977) was that it delayed flow separation at higher angles of attack, and a stall did not occur abruptly. For Newman *et al* (1977), the pleats have no aerodynamic significance, and the main contributors to the enhanced lift are attributed to the spurs, or microscopic hair-like features, and serrations found on the leading edge. These microscopic features lie within the boundary layer as they are of the order of micrometers, and can potentially serve to trip the flow to enhance the transition to turbulent flow.

However, these conclusions are in contrast to those of Buckholz (1986) who tested a pleated wing model at $Re_c = 1500$ and concluded that the pleated configuration increases lift. Wakeling and Ellington (1997a) also come to the same conclusion when filming free gliding dragonflies and conducting wind tunnel experiments on their wings at a Reynolds number ranging from 700 to 2400. $C_{L\max}$ recorded for free gliding dragonflies was 0.93 and 1.07 when tested in a wind tunnel environment. Wakeling and Ellington (1997a) stated that the enhanced lift produced by dragonflies is not attributed to the Reynolds number, the aspect ratio or the wing area, but rather a surface feature, mainly the corrugations found in dragonflies.

Other comprehensive wind tunnel experiments on pleated airfoils compared to technical airfoils were conducted by Okamoto *et al* (1996) and Kesel (2000). Okamoto *et al* (1996) conducted several detailed experiments to investigate the aerodynamic characteristics of dragonfly wings and model wings at a Reynolds number ranging from 11 000 to 15 000. Their experiments consisted of force and moment measurements in a horizontal wind tunnel, auto-rotational flights in a vertical wind tunnel and gliding flight in still air. The effects of thickness, camber, pleats and leading edge sharpness were all tested using various models to examine the lift curve slope, maximum lift coefficient, minimum drag coefficient and lift-to-drag ratio. From their experiments, a thinner flat plate with camber and a sharp leading edge is the profile that provides the best lift at these low Reynolds numbers. The tests also indicated that the pleated plate outperformed the flat plate at all angles of attack. The orientation of the leading edge of the pleated plate had a significant effect on the lift generated at high angles of attack. Okamoto *et al* (1996) concluded that a downward facing

leading edge had a much better performance than an upward facing leading edge. Experimental tests on actual dragonfly wings from an *Anax parthenope julius* produced a $C_{L\max}$ of 1.05, which was higher than that produced by streamlined airfoils.

Kesel (2000) extracted three cross-sections at different positions along the span of a wing of an *Aeschna cyanea* to develop the pleated models. The aerodynamic performance of the pleated models was compared to its corresponding profiled airfoil at a chord Reynolds number of 10 000, and the results showed that the pleated airfoils generated higher lift than the profiled airfoils. Pressure measurements performed on a model that represented the front portion of a pleated airfoil showed that a net negative pressure sufficient to produce lift occurred only at angles of attack greater than 0°. However, unlike Okamoto *et al* (1996), Kesel (2000) revealed that the orientation of the leading edge does not have an effect in enhancing the lift production. As with the early flow visualization experiments, Kesel (2000) noticed trapped vortices present in the folds that serve to change the effective profile of the airfoil. Yet, according to Kesel (2000), it is the camber found in dragonfly wings that is preserved even though trapped vortices are present in the folds. Kesel (2000) stated that an increase in lift did not arise by simply placing uniform or randomly spaced corrugations along the chord of an airfoil (Buckholz 1986); rather the airfoil must be finely tuned, a function innate to nature.

The pleated wing provides a structural benefit, allowing for a low mass yet stiff structure, but the question remains as to what precisely is the effect of the pleated structure on the wing aerodynamics. With the advent of micro-aerial vehicles (MAVs), it has become clear that there is much that can be learned from insect flight that could be translated into engineered systems. For fixed wing MAVs, wings that simultaneously provide a superior aerodynamic performance and structural robustness are critical. Thus, if it is found that the pleats have an aerodynamic benefit, then such wings could be candidates for micro-aerial vehicles and this is the primary motivation for the current computational study.

The objective of the current research is to use numerical simulations to examine the aerodynamic performance of a pleated airfoil inspired from a cross-section of the forewing of a dragonfly (*Aeshna cyanea*). In order to provide some perspective for the performance of the pleated airfoil, simulations are performed of flow past its smoothed counterpart (profiled airfoil), and a flat plate in gliding flight, at chord Reynolds numbers ranging from 500 to 10 000, and angles of attack ranging from 0° to 10°. These parameter ranges are relevant for both dragonflies and micro-aerial vehicles. Past experimental studies (Buckholz, 1986, Okamoto *et al* 1996, Kesel, 2000) have found no intrinsic three-dimensional effects at these low Reynolds numbers. Thus, 2D simulations are implemented in this study to encompass a relatively wide range of the parameter space necessary to draw some general conclusions regarding pleated airfoils. It should be noted that all computational studies of the dragonfly wing performance to date (Gustafson and Leben 1991, Wang 2000, Mittal *et al* 2002, Lentink and Gerritsma 2003, Isogai *et al* 2004, Sun and Lan 2004) have focused on flapping flight and have employed wing models which are smooth.

2. Numerical method

The solver used in the current investigation employs a Cartesian grid method wherein flow past immersed complex geometries can be simulated on non-body conformal Cartesian grids (Najjar and Mittal 2003, Mittal *et al* 2004, 2007, Dong *et al* 2006). In addition to these references, further details regarding immersed boundary methods can be found in Ye *et al* (1999), Udaykumar *et al* (2001), Mittal and Iaccarino (2005). Here we provide a brief overview of the current method.

2.1. Governing equations

The equations governing the flow in the numerical solver are the time-dependent, viscous incompressible Navier–Stokes equations. The momentum and continuity equations are as follows:

$$\frac{\partial u_i}{\partial x_i} = 0 \tag{1}$$

$$\frac{\partial u_i}{\partial t} + \frac{\partial (u_i u_j)}{\partial x_j} = -\frac{1}{\rho}\frac{\partial P}{\partial x_i} + \nu \frac{\partial}{\partial x_j}\left(\frac{\partial u_i}{\partial x_j}\right), \tag{2}$$

where the indices, $i = 1, 2, 3$, represent the x-, y- and z-directions, respectively, and the velocity components u_1, u_2 and u_3 correspond to u, v and w respectively. The equations are non-dimensionalized with the appropriate length and velocity scales, in this case the airfoil chord and freestream velocity. Hence, the tensor equations in (2) are written as

$$\frac{\partial u_i}{\partial t} + \frac{\partial (u_i u_j)}{\partial x_j} = -\frac{\partial P}{\partial x_i} + \frac{1}{Re}\frac{\partial^2 u_i}{\partial x_j \partial x_j}, \tag{3}$$

where Re corresponds to the Reynolds number.

The non-dimensional form of the Navier–Stokes equations is discretized using a cell-centered, collocated (non-staggered) arrangement where all variables (i.e. velocity components and pressure) are located at the same physical location. The equations are integrated in time using the fractional step method (Chorin 1967). In the first sub-step of this method, a modified momentum equation is solved and an intermediate velocity is obtained. A second-order Adams–Bashforth scheme is implemented for the convective terms, while the diffusion terms are discretized with an implicit Crank–Nicolson technique which eliminates the viscous stability constraint. The second step of the fractional step method is the solution of a pressure correction equation by solving a Poisson equation. A Neumann boundary condition is implemented on this pressure correction step at all boundaries. The Poisson equation, being the most time-consuming part of the solution algorithm, is solved with a flexible and efficient geometric multi-grid algorithm with a flexible semi-coarsening strategy (Schaffer 1998, Piquet and Vasseur 2000) which employs a Gauss–Siedel line-SOR (successive overrelaxation) smoother. Performance tests of the multi-grid method have been carried out by Bozkurttas *et al* (2005).

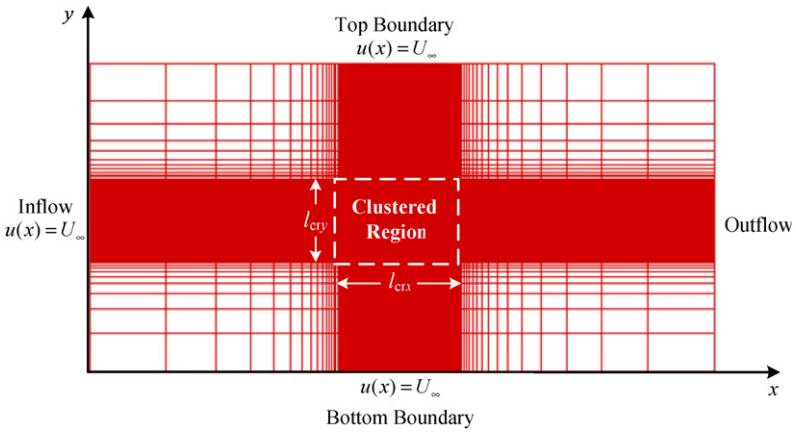

Figure 2. A typical two-dimensional, non-uniform Cartesian grid with prescribed boundary conditions used in the numerical simulations. The airfoils are placed inside the clustered region which contains high grid resolution of dimensions l_{crx} and l_{cry} representing the lengths in the x- and y-directions respectively.

The basic concept of the current immersed boundary method is to compute the flow variables for the ghost cells (GC), such that boundary conditions on the immersed boundary in the vicinity of the ghost cells are satisfied while preserving second-order accuracy. Ghost cells are those cells whose centers lie inside the immersed body and have at least one neighboring cell which lies outside the immersed body. The process begins by generating a non-conformal Cartesian grid followed by the specification of the immersed boundary, which comprise a number of densely spaced marker points connected by linear segments. A procedure that identifies the fluid cells, solid cells and ghost cells is then implemented.

2.2. Boundary conditions

The two-dimensional domains implemented in the current study consist of four boundary conditions located at left, right, top and bottom of the computational domain, as shown in figure 2. A constant inflow velocity (U_∞) of unity normal to the boundary was imposed on the left side of the domain, and the right edge of the domain was set to an outflow boundary where the gradient values are set to zero. A Dirichlet boundary condition was applied to the top and bottom boundaries with a u-velocity equal to U_∞ and the v-velocity component was set to zero. For this reason, the top and bottom boundaries must be set to a large distance away from the immersed body to minimize the effects of the boundary condition on the flow near the geometry.

2.3. Validation case

In order to validate the current numerical solver, simulations of flow past a NACA 0008 airfoil were performed and compared to the published results of Kunz and Kroo (2001). Four validation cases were conducted using a NACA 0008 airfoil at angles of attack of 0 and 4° with chord Reynolds numbers (Re_c) of 2000 and 6000. The simulations were performed on a 926 × 211 ($N_x \times N_y$) non-uniform Cartesian grid with domain sizes of $6.5c \times 3.5c$ and $12.0c \times 9.0c$ for the 0 and 4° angle-of-attack cases respectively. The computational domain used in the validation case at $\alpha = 4°$ is shown in figure 3. The

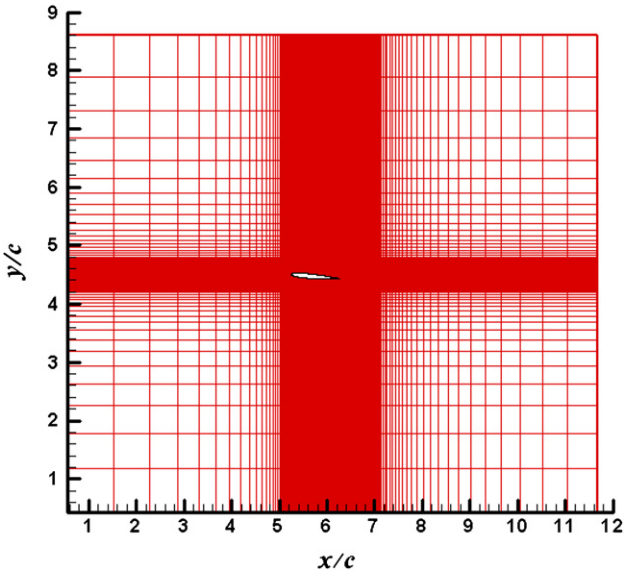

Figure 3. Computational domain with a non-uniform Cartesian grid of 926 × 211 used in the validation case of a NACA 0008 airfoil at 4° with Reynolds numbers of 2000 and 6000.

domain dimensions and grid sizes were based on a sequence of simulations, which examined the effect of these factors on the results (Vargas 2006).

The results of interest in this particular validation case were the lift and drag coefficients at the two angles of attack. The numerical results displayed in table 1 are time-averaged lift and drag values averaged from a non-dimensionless time, tU_∞/c, between 5 and 20 and between 10 and 20 for the airfoils at $\alpha = 0°$ and 4° respectively. Table 1 shows a near-zero lift coefficient obtained numerically as expected for the NACA 0008 airfoil at an $\alpha = 0°$, while the difference in the drag coefficient is no more than 3.5%, which is an acceptable value. A lesser percentage difference was obtained at $\alpha = 4°$, in which C_L and C_D varied no more than 1.15% for $Re_c = 2000$ and 6000. Overall, the numerical results are in good agreement with those obtained by Kunz and Kroo (2001) for both angles of attack

Table 1. Comparison of the numerical C_L and C_D with the results from Kunz and Kroo (2001) for NACA 0008 at $\alpha = 0^\circ$ and 4° with $Re_c = 2000$ and 6000.

	$\alpha = 0^\circ$				$\alpha = 4^\circ$			
	$Re_c = 2000$		$Re_c = 6000$		$Re_c = 2000$		$Re_c = 6000$	
	C_L	C_D	C_L	C_D	C_L	C_D	C_L	C_D
Numerical results	0.0005	0.0785	0.0003	0.0441	0.2732	0.0812	0.2396	0.0469
Kunz and Kroo (2001)	–	0.0760	–	0.0426	0.2719	0.2369	0.2369	0.0465
Percentage difference	–	3.28%	–	3.50%	0.48%	0.99%	1.15%	0.82%

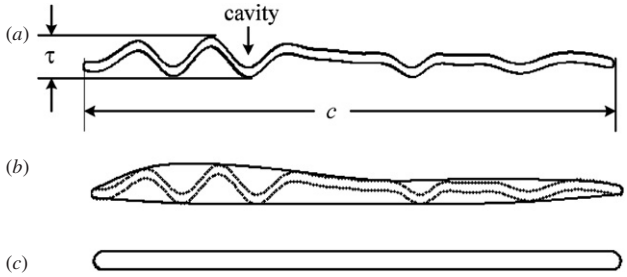

Figure 4. The two-dimensional airfoils used in the numerical simulation. (*a*) Pleated airfoil representing a cross-section of the forewing of a dragonfly (*Aeshna cyanea*) having $\tau/c = 7.531\%$, (*b*) profiled airfoil with $\tau/c = 7.531\%$ obtained by connecting the local extrema found in the pleated airfoil and (*c*) flat plate with $\tau/c = 3.342\%$.

and chord Reynolds numbers. This validation case clearly demonstrates that the current immersed boundary solver is capable of accurately simulating flow past airfoils at these low Reynolds numbers on a non-uniform Cartesian grid.

2.4. Airfoil geometries

The pleated airfoil implemented in the numerical simulation corresponds to a cross-section located at the mid-section of the forewing of a dragonfly (*Aeshna cyanea*). The specific profile chosen for the numerical simulations corresponds to 'Profile 2', which was digitally extracted from the paper of Kesel (2000). From the three pleated geometries to select from the paper of Kesel (2000), 'Profile 2' was chosen due to its horizontal leading edge, thus eliminating the issue that the orientation of the leading edge has an influence on the aerodynamic performance (Okamoto *et al* 1996). For the purposes of reducing the resolution requirements in the simulation, the sharp edges of the pleats were rounded out slightly without affecting the basic geometry of the pleats and the overall shape of the airfoil. For complete details on the construction of the pleated airfoil, the reader is referred to Vargas (2006).

The second airfoil referred to as a 'profiled' airfoil represents a streamlined airfoil constructed by fitting a spline through the local extrema of the dragonfly wing section as shown in figure 4. This airfoil represents the hypothetical scenario if a dragonfly was able to have enough material to form a streamlined shape. A hypothetical streamlined insect wing, if it exists, would require truss-like members connecting the top and bottom surfaces to give the wing some rigidity, thus adding additional weight. The purpose of the profiled airfoil is to see what benefits are gained from streamlining when this airfoil operates at ultra-low Reynolds numbers.

Finally, a flat plate with rounded leading and trailing edges, representing the simplest airfoil, was also included as a baseline case representing a flat airfoil without pleats. For comparison purposes, all length scales used in the experiments of Kesel (2000) were incorporated in the design of the geometries. Figure 4 shows the cross-section of the geometries used in the numerical study with a τ/c ratio of 7.531% for the pleated and profiled airfoils and a τ/c ratio of 3.342% for the flat plate, where τ is the thickness and c is the chord length. The thickness of the plate corresponds to the thinnest section of the profiled airfoil which is located near the leading edge.

2.5. Computational domains

The grid resolution and the size of the domain are two important parameters to be aware of when performing such simulations. The objective when generating a Cartesian grid is to provide adequate resolution to accurately compute the flow variables. It is also desirable that the domain boundaries be far enough from the airfoil so that the boundary effects are minimal. Three computational domains were developed to accommodate the three airfoils at an angle of attack of 0, 5 and 10°.

Grid refinement and domain independence studies were conducted at $Re_c = 10\,000$ to ensure that the computational domain had enough grid resolution and wase large enough to minimize the influence of the boundaries with the flow near the vicinity of the airfoils. Grids and domains were deemed acceptable if further changes in either one of these produced less than a 5% change in the mean shear and pressure forces (lift and drag) on the foil. Further details of this refinement study can be found in Vargas (2006). Mean velocity profiles in the wake were also compared, and we ensured that these also did not change to any significant degree with changes in the grid. Presented in table 2 is a summary of the domain and grid sizes that were finally used for the various cases simulated in the current study. Figure 5 shows the grid in the vicinity of the leading edge of the pleated airfoil and it shows the high resolution provided to the region around the pleats. The simulations in the current study have been run for 15, 20 and 40 chord flow time units for the airfoils at $\alpha = 0^\circ$, 5° and 10° respectively. These chord flow time units were adequate to obtain a statistically stationary state for all cases simulated. The numerical simulations were carried out with a uniform

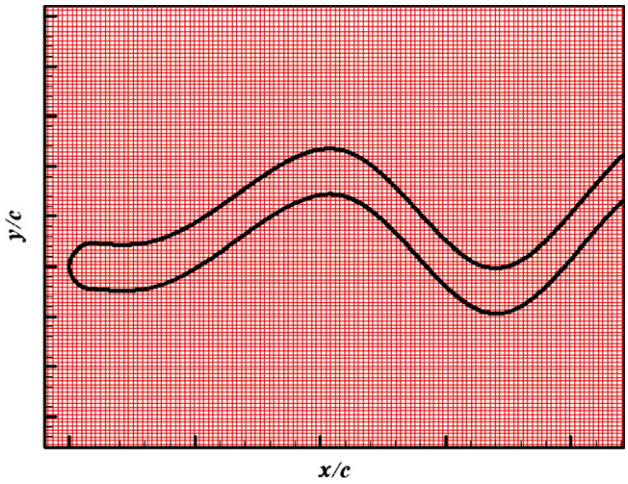

Figure 5. Close-up view of grid in the vicinity of the leading edge showing the high resolution provided to the pleats.

Table 2. Summary of the three computational domains with different chord Reynolds numbers used for the numerical simulations at $\alpha = 0^\circ$, 5° and 10°.

Angle of attack	Domain size	Grid size	Chord Reynolds no. (Re_c)
$\alpha = 0^\circ$	$6.5c \times 3.05c$	926×211	10 000 and 5000
$\alpha = 5^\circ$	$12.0c \times 9.0c$	926×211	10 000, 5000 1000 and 500
$\alpha = 10^\circ$	$12.0c \times 27.0c$	771×251	10 000 and 5000

time step of $0.0002c/U_\infty$ which maintained the CFL under the stability limit.

3. Results

The evaluation of results begins at $Re_c = 10\,000$ because several gliding flight experiments pertaining to dragonfly wing sections have been conducted at this Reynolds number. Experimental studies on the steady-state aerodynamics of dragonfly wings conducted by Newman *et al* (1977) and Okamoto *et al* (1996) have used a chord Reynolds number of the order of 10^4. Kesel's experimental studies were also conducted at $Re_c = 10\,000$, and because the pleated geometry was replicated from Kesel (2000), this serves as a way to compare the numerical results with published data. Before proceeding to the discussion of the results, a critical assessment of the numerical result was performed.

3.1. Critical assessment of computed results

Using the same flow parameters and geometrical dimensions as Kesel (2000), this allowed for validation and a critical analysis of the numerical results. The key quantities examined are the lift and drag coefficients which are defined as

$$C_L = \frac{F_L}{1/2\rho U_\infty^2 c}, \qquad C_D = \frac{F_D}{1/2\rho U_\infty^2 c}. \tag{4}$$

The time histories of C_L and C_D for the airfoils at $Re_c = 10\,000$ and $\alpha = 0^\circ$ are shown in figure 6, and it can be seen that

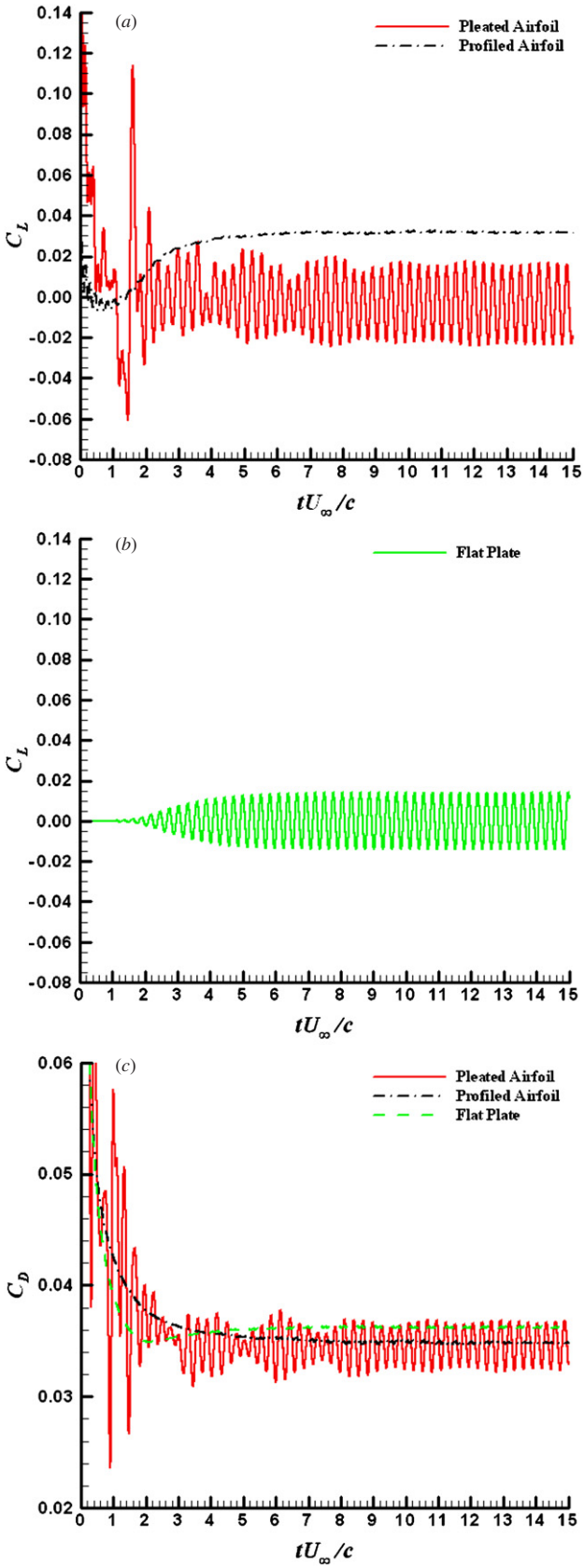

Figure 6. Time history of C_L (*a*) pleated and profiled airfoils, (*b*) flat plate and (*c*) C_D for all airfoils at $\alpha = 0^\circ$ and $Re_c = 10\,000$.

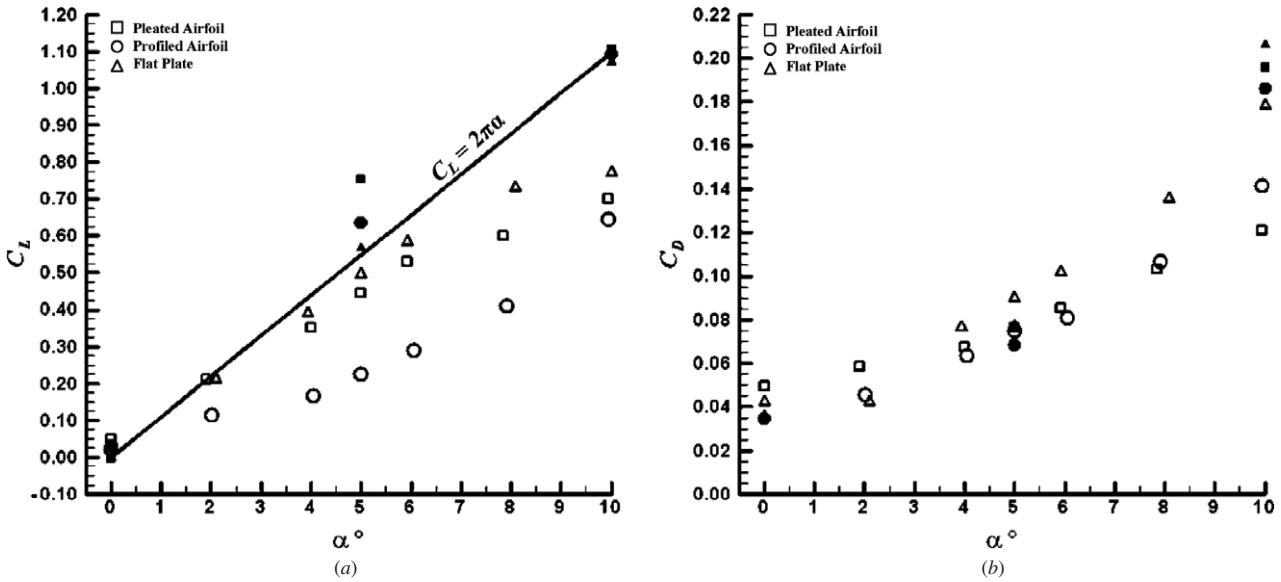

Figure 7. Comparison between the numerical (solid symbols) and the experimental force coefficients of Kesel (2000) (open symbols) for $Re_c = 10\,000$ and various angles of attack. (*a*) Lift coefficient, (*b*) drag coefficient. The theoretical lift is also plotted for comparison purposes.

Table 3. The comparison of the numerical and experimental (Kesel 2000) mean force coefficients for airfoil geometries at $\alpha = 0^\circ$ and $Re_c = 10\,000$.

Airfoil geometry	Numerical				Experimental		Blasius flat plate
	C_L	C_{Ds}	C_{Dp}	C_D	C_L	C_D	C_{Ds}
Pleated airfoil	−0.003	0.008	0.026	0.035	$0.053 \pm 3.71 \times 10^{-4}$	$0.049 \pm 1.27 \times 10^{-3}$	–
Profiled airfoil	0.032	0.023	0.012	0.035	$0.016 \pm 1.12 \times 10^{-4}$	$0.040 \pm 1.04 \times 10^{-3}$	–
Flat plate	0.000	0.024	0.013	0.036	$0.022 \pm 1.98 \times 10^{-4}$	$0.041 \pm 1.07 \times 10^{-3}$	0.0266

each airfoil has a distinct time history. For instance, it is seen that whereas the profiled airfoil reaches a steady state, both the pleated and the flat plate airfoils attain an oscillatory state. The mean values of the force coefficients are computed after a stationary state is reached for this and other cases, and here, a comparison between the numerical results and those of Kesel (2000) at $Re_c = 10\,000$ is performed. The experimental lift and drag coefficients were obtained from the graphs provided in the work of Kesel (2000) using Plot Digitizer 2.4.0, a Java program that allows for data extraction from scanned images.

The comparison between the numerical and the experimental C_L in figure 7 show noticeable discrepancies between the two results. For example, the experimental results show that the flat plate produces the most lift at $\alpha = 5^\circ$, whereas the numerical results reveal that the pleated airfoil produces the most lift. Also, a greater variation in the lift and drag coefficients is observed at $\alpha = 10^\circ$ in the experiments. A reasonable agreement in the drag coefficient of the pleated and the profiled airfoils is observed only at $\alpha = 0^\circ$ and 5°.

Focusing on the results at $\alpha = 0^\circ$, as seen in table 3, one again observes that the numerical results are not entirely consistent with the experimental results of Kesel (2000). The data in table 3 display the mean C_L and C_D coefficients along with the drag component due to shear stress and pressure denoted by C_{Ds} and C_{Dp} respectively, which were averaged beyond 5 time units in order to eliminate the transitory effects. As shown in table 3, the CFD shows that the profiled airfoil produces the most lift and the computed value is about two times greater than the experimentally measured C_L. Furthermore, the experimental results indicate that the pleated airfoil section generates more than three times the lift of the profiled airfoil.

Comparing the drag coefficient at $\alpha = 0^\circ$ also shows differences between the two datasets. The experimental results of Kesel (2000) reveal that the pleated airfoil generates the most drag when compared to the flat plate and the smoothed airfoil. The CFD-based drag corresponding to the profiled airfoil and the flat plate is within 11% of the experimental results of Kesel (2000).

The tabulated C_L values in table 3 provide some indication regarding the relative accuracy of the experimental and numerical forces. The numerical simulations yield a zero mean lift coefficient for the flat plate, whereas the experiments measured a lift coefficient for the flat plate of 0.022, which is greater than that measured for the profiled airfoil. This seems to indicate a significant anomaly in the experiment since a flat plate at 0° angle of attack should not produce any lift and certainly not more than that of a non-symmetric airfoil. It is also noted that the numerical C_L of the flat plate is closer to the theoretical lift defined as $C_L = 2\pi\alpha$ for all angles of attack,

Table 4. Comparison between the theoretical and numerical skin friction, where the theoretical c_{ds} was obtained using the Blasius solution for a flat plate, $C_{Ds} = 2.656/\sqrt{Re_c}$, at various chord Reynolds numbers.

Chord Reynolds number	Theoretical C_{Ds}	Numerical C_{Ds}	Percentage difference
10 000	0.0266	0.0236	11.12%
5000	0.0376	0.0339	9.64%
1000	0.0840	0.0879	4.65%

whereas the experimental lift varies significantly from this value. This in our view indicates that the experimental results are significantly modified by end effects from the tunnel walls and that this effect becomes even more pronounced at higher angles of attack.

Another analysis used to further verify the numerical results is to compare the numerical skin friction or shear drag defined as $C_{Ds} = \int (\tau_s, \cdot n)\, \mathrm{d}s$ of the flat plate to the Blasius solution for a flat plate which assumes a thin plate of infinite length at zero incidence. Comparing the numerical skin friction to the Blasius solution at zero incidence with $Re_c =$ 10 000 results in an 11.12% lower value, as seen in table 4. This arises from the fact that the flat plate has rounded leading and trailing edges where shear stress contribution to drag is lower. It should be pointed out that when the chord Reynolds number is lowered and no flow separation occurs at the trailing edge, the percentage difference between the numerical and theoretical skin friction reduces to less than 5%, demonstrating the accuracy and reliability of the numerical results. As mentioned before, extensive grid refinement and domain independence studies were conducted such that the results were independent of the grid density and domain size. Also, the validation case performed on the NACA 0008 airfoil yields a percentage difference in C_D and C_L of less than 3.5% for all angles of attack and chord Reynolds numbers that were tested.

The above critical assessment of the numerical results along with the grid and domain refinement studies provides sufficient confidence in the fidelity of the numerical simulations. Possible sources of inaccuracy in the experiments of Kesel (2000) could be the difficulty of measuring small forces at a low chord Reynolds number and of maintaining a two-dimensional flow across the wind tunnel model, given that their model had a spanwise aspect ratio of only 3.469. No discussions of these aspects have been provided in the paper of Kesel (2000).

3.2. Effect of angle of attack

The first step in understanding the aerodynamic performance of the pleated airfoil was to perform an analysis at $\alpha = 0^\circ$ at a chord Reynolds number of 10 000 and 5000. The mean force coefficients pertaining to their respective airfoil geometry are tabulated in table 5. At zero incidence, the drag production leads to some interesting observations. As expected, the overall drag coefficient of each airfoil increases as Re_c is decreased because the viscous effects are more dominant at lower Reynolds numbers which cause the skin friction to be the major contributor to the overall drag. The profiled airfoil and flat plate produce shear drag that constitutes about 65% and 71% of the total drag at $Re_c = 10\,000$ and 5000, respectively. In contrast, the shear drag for the pleated airfoil is about 24% and 31% of the total drag at $Re_c = 10\,000$ and 5000 correspondingly.

To understand the effect of the airfoil shape on shear drag, the shear drag distribution on the suction and pressure side of the airfoils at $Re_c = 10\,000$ and 5000 are plotted in figure 8. As seen in the figure, the shear drag distribution at both Re_c follows the same trend with all airfoils experiencing a sharp increase in shear drag at the leading edge. The profiled airfoil generates most of its shear drag on the upper surface near the leading edge between $0.0 \leqslant x/c \leqslant 0.25$ and there is another region of some shear drag production near the trailing edge between $0.65 \leqslant x/c \leqslant 1.0$. In contrast, the flat plate generates nearly even drag over its entire suction and pressure surface.

The shear drag distribution of the pleated airfoil is significantly more complex due to the complexity of the airfoil geometry. In particular, there are large peaks of shear drag that are located near the peak of the corrugations on both the suction and the pressure surface. However, most interesting is the appearance of large regions of *negative* shear drag in the intervening spaces. Thus, it becomes clear that the low shear drag of the pleated airfoil is due to these negative shear regions which negate the effect of positive shear drag in the other regions of the foil.

The origin of the positive and negative peaks in the shear drag becomes clear by examining the mean flow over the airfoil. As seen in figure 9(*a*), the long time-averaged streamlines on the pleated airfoil at $Re_c = 10\,000$ show that there is a trapped vortex in each cavity which causes the overall flow to resemble that past the profiled airfoil. This observation is in line with the experimental studies of Rees (1975b), Newman *et al* (1977) and Rudolph (1977), who hypothesized that flow would behave in such a way due to the trapped vortex inside each cavity. Furthermore, the flow

Table 5. Comparison of the mean aerodynamic coefficients for airfoil geometries at $\alpha = 0^\circ$ at $Re_c = 10\,000$ and 5000. The averages were computed beyond 5 time units in order to eliminate the transient portion of the flow.

Airfoil geometry	$Re_c = 10\,000$				$Re_c = 5000$			
	C_L	C_{Ds}	C_{Dp}	C_D	C_L	C_{Ds}	C_{Dp}	C_D
Pleated airfoil	−0.003	0.008	0.026	0.035	0.008	0.015	0.032	0.047
Profiled airfoil	0.032	0.023	0.012	0.035	0.028	0.035	0.015	0.050
Flat plate	0.000	0.024	0.013	0.036	0.000	0.034	0.014	0.047

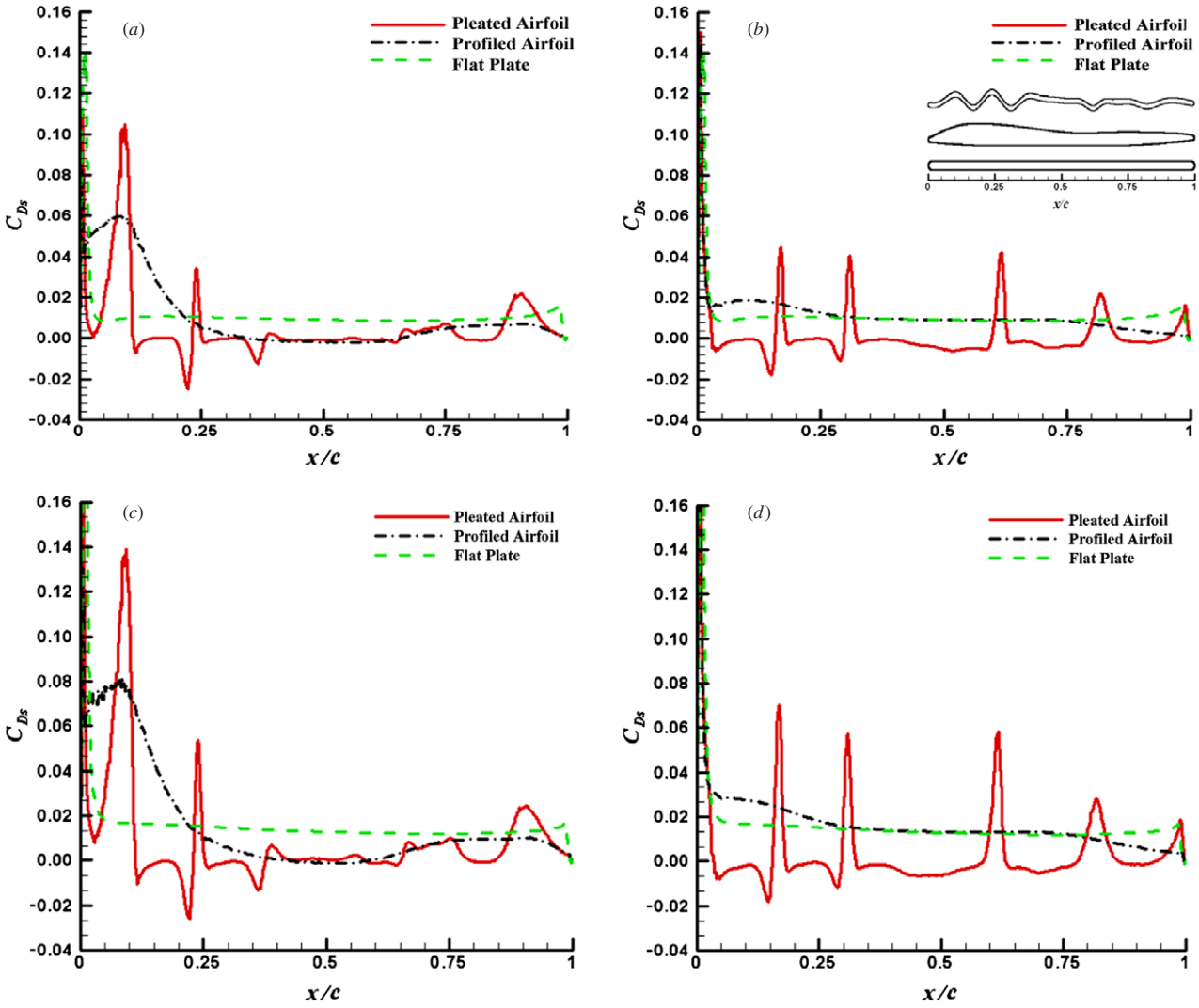

Figure 8. Shear drag distribution along the suction and pressure surface of the airfoils at $\alpha = 0^\circ$. (*a*) $Re_c = 10\,000$, suction surface. (*b*) $Re_c = 10\,000$, pressure surface. (*c*) $Re_c = 5000$, suction surface. (*d*) $Re_c = 5000$, pressure surface.

separates just downstream of the tip of each corrugation and reattaches just upstream of the tip of the next corrugation. As described in figure 9(*b*), the region between the separation and reattachment points is a region with a recirculating flow and there is negative shear drag generated in this region. In addition, the positive and negative peaks in the shear drag occur near the flow reattachment point as indicated in figure 9 since these are the regions where the surface normal gradient in the tangential velocity is large. The pleated airfoil is therefore able to produce total drag comparable to that of its smooth counterpart by reducing the shear drag as a direct result of flow reversal occurring in each cavity.

Comparing the shear drag at each angle of attack as seen in figure 10, one observes that the pleated airfoil produces the least amount of shear drag at all angles of attack and the two chord Reynolds numbers employed. The shear drag for the profiled airfoil is nearly constant between 0 and 5° but decreases as the angle of attack is increased to 10°. However, as expected, an increase in the shear drag is observed for all airfoils as the chord Reynolds number is reduced to 5000.

3.3. Gliding ratio

The gliding ratio which is the ratio of lift to drag is the key quantity of interest for gliding flight. This quantity is plotted for all the three airfoils at $Re_c = 10\,000$ and 5000 and various angles of attack in figure 11. At $\alpha = 0^\circ$, the profiled airfoil with its non-symmetrical shape produces a non-zero C_L/C_D, whereas the other two airfoils effectively show a zero value. As the angle of attack is increased to 5°, despite its unconventional shape, the glide ratio of the pleated airfoil is slightly higher than the profiled airfoil at $Re_c = 10\,000$, but is significantly higher at $Re_c = 5000$. Note that the pleated airfoil attains a peak glide ratio of about 10 which is quite respectable given the low Reynolds number and unconventional shape. When compared to the flat plate, it is seen that at the intermediate $\alpha = 5^\circ$ case, the flat plate performs better at $Re_c = 5000$

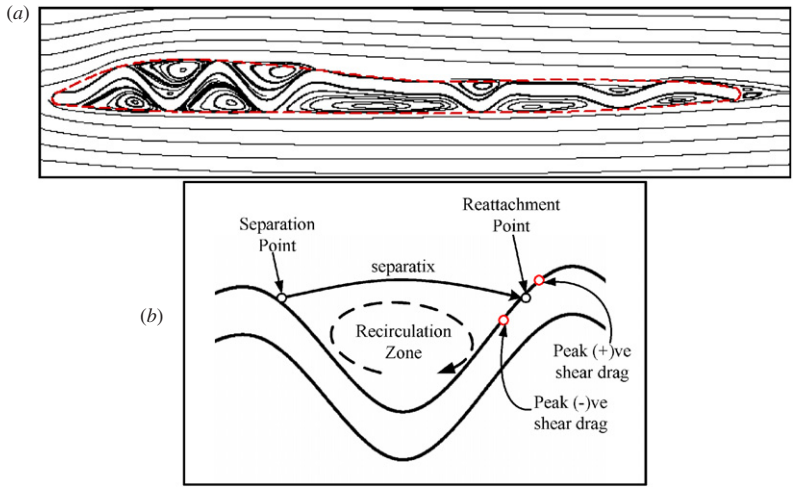

Figure 9. (*a*) Time-averaged streamlines generated by the pleated airfoil at $Re_c = 10\,000$ with the outline of the profile airfoil depicted by dashed lines superimposed to demonstrate that the flow looks as if it pertains to this airfoil. (*b*) Schematic showing the correspondence of surface shear with the flow pattern in typical corrugation.

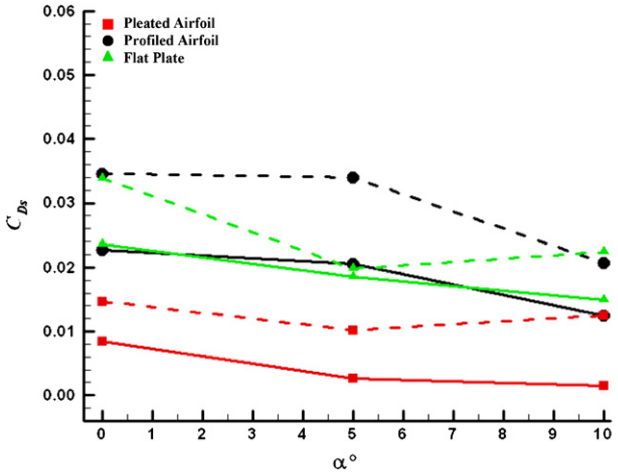

Figure 10. The mean shear drag of the pleated airfoil, profiled airfoil and flat plate with varying angles of attack at $Re_c = 10\,000$ (solid lines) and $Re_c = 5000$ (dashed lines).

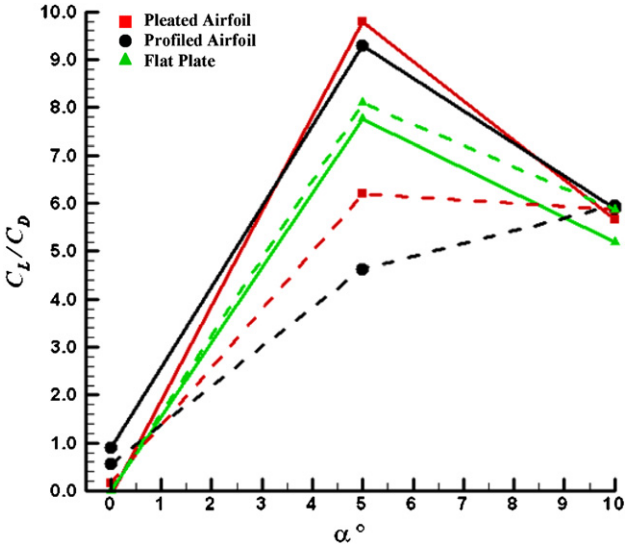

Figure 11. The comparison of the aerodynamic performance (C_L/C_D) of the pleated, profiled and flat plate airfoils at $Re_c = 10\,000$ and 5000 represented by the solid and dashed lines respectively.

whereas the pleated airfoil is significantly better at $Re_c = 10\,000$.

At $\alpha = 10^\circ$ with $Re_c = 10\,000$, a decline in the performance of all airfoils is observed, indicating that all these airfoils stall between 5° and 10° angles of attack. For the lower Reynolds number case, both the pleated and the flat plate airfoils show a stall behavior whereas the profiled airfoil show a further increase suggesting that the stall angle at this Reynolds number for this airfoil is beyond 10°.

3.4. Effect of the Reynolds number

It is important to examine the effect of the Reynolds number on the foil performance since this has implications of how well these wings would work for dragonflies (and MAVs) of different sizes. This issue is also important from the point of view of use of such wings in micro-aerial vehicles. Therefore, a numerical study which focuses on the effect of the Reynolds number on the foil performance was conducted. For this study, the intermediate angle of attack of $\alpha = 5^\circ$ was chosen where the best performance was observed for the pleated foil. At this angle of attack, simulations at $Re_c = 1000$ and 500 were performed in addition to $Re_c = 5000$ and 10 000 simulations that have already been described in the previous sections.

Figure 12 shows the time mean streamlines for all the airfoils at the various Reynolds numbers studied here. The plots show that at this angle of attack, large regions of separation exist over all the airfoils for Reynolds numbers greater than 5000. Below this Reynolds number, the flow over the airfoils is mostly attached and does not show large regions

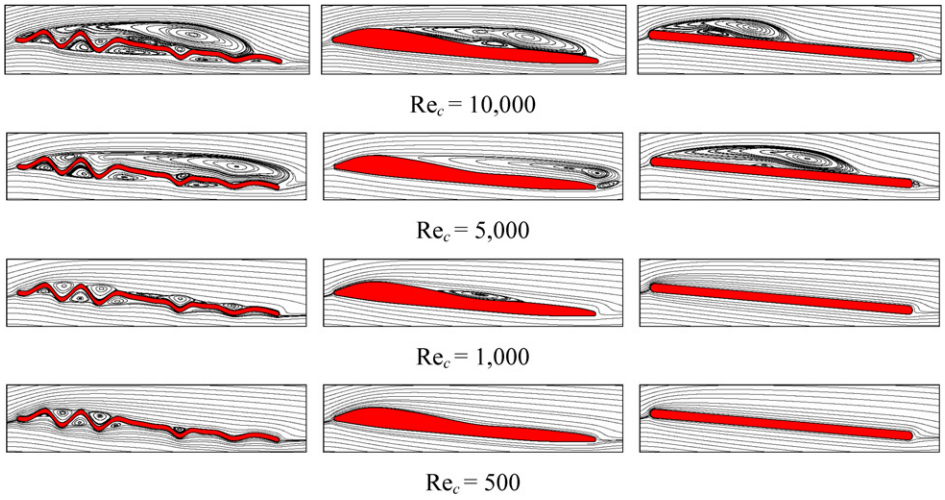

Figure 12. Time-averaged streamlines of the pleated airfoil (left), profiled airfoil (middle) and flat plate (right) at $\alpha = 5^\circ$ with $Re_c = 10\,000$, 5000, 1000 and 500.

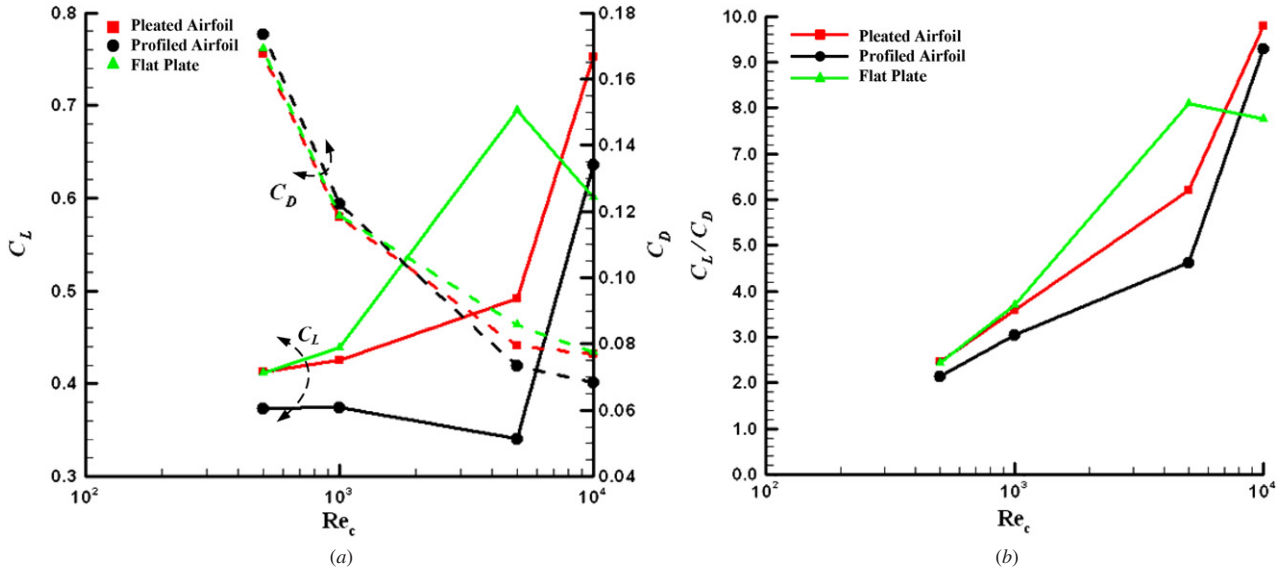

Figure 13. (*a*) The mean lift and drag coefficients of the three airfoils with varying chord Reynolds numbers. Solid and dashed lines represent C_L and C_D respectively. (*b*) Lift-to-drag ratio versus the chord Reynolds number for the airfoils at $\alpha = 5^\circ$.

of separation. Furthermore, when $Re_c = 5000$ and 10 000 cases are compared, the separation is much more extensive at the lower Reynolds numbers. Thus, a further increase in the Reynolds number beyond this value tends to reduce the extent of separation.

A comparison of the time-mean force coefficient with varying chord Reynolds numbers is shown in figure 13. At $Re_c = 500$, the flat plate and the pleated airfoil produce the same C_L of about 0.41. The lift for the pleated and profiled airfoils is seen to be constant from $Re_c = 500$–1000, while the lift of the flat plate increases between this range. Increasing the chord Reynolds number by a factor of 5 from 1000 causes the lift of both the plate and the pleated airfoils to increase, and the lift of the profiled airfoil to decrease slightly. The flat plate experiences a greater rate of increase, and generates the most C_L when compared to the other airfoils at $Re_c = 5000$. A rapid increase in the lift for the pleated and profiled airfoils occurs at $Re_c = 10\,000$, but the lift associated with the flat plate is observed to decrease. Analyzing the coefficient of drag, one observes that the viscous effects are dominant at a Reynolds number below 1000 and the drag production for all airfoils is nearly the same. At higher Reynolds numbers, some differences in the drag coefficient for the three airfoils with the pleated foil producing drag which is intermediate to the profiled and flat plate airfoils are observed.

The effect of the Reynolds number on the gliding ratio is shown in figure 13. As seen in the figure, at Re_c less than 1000, the flat plat and the pleated airfoils have about nearly equal C_L/C_D, and as Re_c increases to 5000, the flat plate has the best performance. However, the flat plate experiences a decline in performance beyond $Re_c = 5000$, while C_L/C_D of the pleated and profiled airfoils keep increasing monotonically.

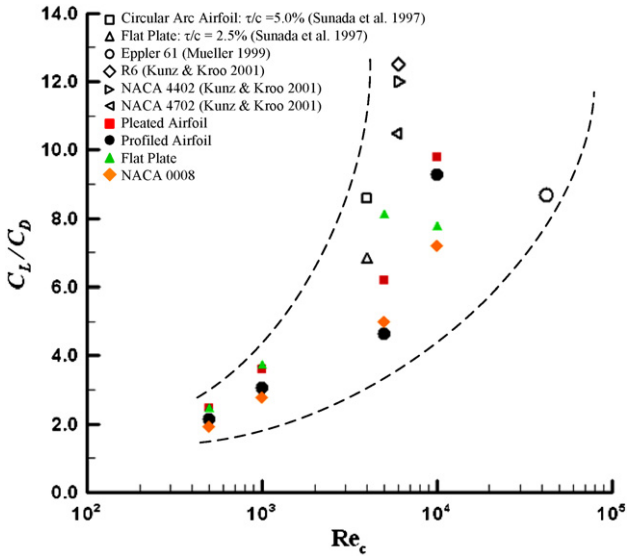

Figure 14. Comparison of the aerodynamic performance of the pleated airfoil, profiled airfoil and flat plate to other engineered airfoils at $\alpha = 5^\circ$ in the low Reynolds number regime.

Figure 13 also shows that the pleated airfoil outperforms the profiled airfoil at all chord Reynolds numbers tested. Thus, the pleated airfoil has two key favorable properties: first, unlike the flat plate, its glide ratio increases monotonically over a large range of Reynolds numbers extending from 1000 to 10 000 and, second, it outperforms the profiled airfoil over this entire range of Reynolds numbers.

Finally, figure 14 compares the glide ratio of the current airfoils with other airfoils at these low Reynolds numbers to provide some context to the aerodynamic performance of the dragonfly wing. Included in this plot are the flat plate, circular arc and NACA airfoils as well as low (Eppler 61) and ultra-low Reynolds number airfoils such as R6 of Kunz and Kroo (2001). The plots show that the glide ratio ranges from about 2 at the lowest Reynolds number of 500 to about 12 at $Re_c = \mathrm{O}(10^4)$. Furthermore, the performance of the pleated airfoil lies somewhere in the middle of the range as denoted by the two dashed lines. Thus, the dragonfly's pleated airfoil, despite being highly unconventional in shape, provides an aerodynamic performance which is comparable to other more conventional engineered airfoils. This coupled with the fact that such a wing is thin and lightweight while still being structurally stiff likely provides one reason why nature has led to such a design in dragonflies. It also indicates that such a wing would be well suited for use in fixed wing micro-aerial vehicles.

4. Conclusion

Despite the highly corrugated and seemingly non-streamlined shape of the pleated airfoil, it was found to perform (in terms of the lift-to-drag ratio) as well and sometimes slightly better than the profiled airfoil over the entire range of parameters tested. Thus it seems clear that through millions of years of adaptation, dragonflies have developed thin (essentially zero thickness), ultra-light membranous wings that perform at least as well as conventional thick wings during gliding flight. The effect of the pleats on the flow is most evident at low angles of attack, where the flow is basically attached to both surfaces of the wing section. At these angles of attack, although the pleated airfoil experiences an increase in the pressure drag, it is more than compensated by a concomitant decrease in the shear drag. The reduction in the shear drag is due to the fact that there exists recirculation zones inside the cavities formed by the pleats, and these lead to a negative shear drag contribution.

In the three-way comparison between the pleated, profiled and flat plate wing sections, it was found that the flat plate has the best performance at low Reynolds numbers ($Re_c \leqslant 5000$) and low angles of attack ($\alpha \leqslant 5^\circ$). For instance, at $\alpha = 5^\circ$ with $Re_c = 5000$, the flat plate produced C_L/C_D which was about 1.75 and 1.3 times greater than the profiled and pleated airfoils respectively. Beyond this range of Reynolds numbers and angles of attack, the performance of the flat plate deteriorated rapidly due to a massive leading edge stall and the pleated airfoil was found to perform relatively well. For instance at $\alpha = 5^\circ$ and $Re_c = 10\,000$, C_L/C_D of the pleated airfoil was 5% and 32% higher than the profiled airfoil and the flat plate respectively.

As mentioned in the introduction, biologically inspired wings are very relevant in the design of micro-aerial vehicles. In this respect, nature provides a design for ultra-light and structurally robust wings that are suitable at ultra-low Reynolds numbers which can be replicated and incorporated into the micro-aerial vehicle wing design. In addition to the pleated airfoil, the flat plate is also found to be a viable airfoil especially for $Re_c < 5000$. The advantage of a pleated wing over a flat plate wing configuration is that the pleats provide added strength in twisting and bending without adding extra weight.

Acknowledgments

A Vargas was supported by NASA–Harriett G Jenkins Predoctoral Fellowship Grant from NASA. The authors would also like to acknowledge support from ONR Grant N00014-09-1-0897.

References

Alexander D E 1984 Unusual phase relationships between the forewing and hindwings in flying dragonflies *J. Exp. Biol.* **109** 379–83

Azuma A 1992 *The Biokinetics of Flying and Swimming* (Berlin: Springer) pp 138–48

Azuma A, Azuma S, Watanabe I and Furuta T 1985 Flight mechanics of a dragonfly *J. Exp. Biol.* **116** 79–107

Azuma A and Watanabe T 1988 Flight performance of a dragonfly *J. Exp. Biol.* **137** 212–52

Bozkurttas M, Dong H, Mittal R and Najjar F M 2005 Towards numerical simulation of flapping foils on fixed Cartesian grids *43rd AIAA Aerospace Sciences Meeting and Exhibit, AIAA Paper 2005-0081 (Reno, NV)*

Brodsky A K 1994 The aerodynamics of insect flight *The Evolution of Insect Flight* (New York: Oxford University Press)

Buckholz R H 1986 The functional role of wing corrugations in living systems *J. Fluids Eng.* **108** 93–7

Chorin A J 1967 A numerical method for solving incompressible viscous flow problems *J. Comput. Phys.* **2** 12–26
Dong H, Mittal R and Najjar F M 2006 Wake topology and hydrodynamic performance of low aspect-ratio flapping foils *J. Fluid Mech.* **566** 309–43
Ellington C P 1984a The aerodynamic of hovering insect flight: I. The quasi-steady analysis *Phil. Trans. R. Soc.* **305** 1–15
Ellington C P 1984b The aerodynamics of hovering insect flight: II. Morphological parameter *Phil. Trans. R. Soc.* **305** 17–40
Ennos A R 1989 The effect on the optimal shapes of gliding insect and seeds *J. Zool.* **219** 61–9
Gustafson K and Leben R 1991 Computations of dragonfly aerodynamics *Comput. Phys. Commun.* **65** 121–32
Hankin M A 1921 The soaring flight of dragonflies *Proc. Camb. Phil. Soc.* **20** 460–5
Hertel H 1966 *Structure, Form, Movement* (New York: Reinhold) pp 78–87
Isogai K, Fujishiro S, Saitoh T, Yamamoto M, Yamasaki M and Matsubara M 2004 Unsteady three-dimensional viscous flow simulation of a dragonfly hovering *AIAA J.* **42** 2053–9
Kesel A B 2000 Aerodynamic characteristics of dragonfly wing sections compared with technical aerofoil *J. Exp. Biol.* **203** 3125–35
Kunz P J and Kroo H 2001 Analysis and design of airfoils for use at ultra-low Reynolds numbers *Fixed and Flapping Wing Aerodynamics for Micro Air Vehicles Applications: Progress in Astronautics and Aeronautics* vol 195 ed T J Mueller (Virginia: AIAA) pp 35–60
Lentink D and Gerritsma M 2003 Influence of airfoil shape on performance in insect flight *33rd AIAA Fluid Dynamics Conf. and Exhibition, AIAA Paper 2003-3447 (Orlando, FL)*
May M L 1976 Thermoregulation and adaptation to temperature in dragonflies (Odonata: Anisoptera) *Ecol. Monogr.* **46** 1–32
May M L 1978 Thermal adaptation to temperature in dragonflies *Odonatologica* **7** 27–47
May M L 1995 Dependence of flight behavior and heat production on air temperature in the green darner dragonfly *Anax junius* (Odonata: Aeshnidae) *J. Exp. Biol.* **198** 2385–92
Miller P L 1987 *Dragonflies* (New York: Cambridge University Press)
Mittal R, Dong H, Bozkurttas M, Najjar F M, Vargas A and von Loebbecke A 2008 A versatile sharp interface immersed boundary method for incompressible flows with complex boundaries *J. Comput. Phys.* **227** 4825–52
Mittal R and Iaccarino G 2005 Immersed boundary methods *Annu. Rev. Fluid Mech.* **37** 239–61
Mittal R, Najjar F M, Byrganhalli R, Seshadri V and Singh H 2004 Simulation of complex biological flows and flow control problems on Cartesian grids *5th Int. Conf. on Advances in Fluid Mechanics (Lisbon, Portugal)*
Mittal R, Utturkar Y and Udaykumar H S 2002 Computational modeling and analysis of biomimetic flight mechanisms *40th AIAA Aerospace Sciences Meeting and Exhibition AIAA Paper 2002-0865 (Reno, NV)*
Mueller T J 1999 Aerodynamic measurements at low reynolds number for fixed wing micro-air vehicles RTO AVT/VKI *Special Course on Development and Operation of UAVs for Military and Civil Applications* (VKI Belgium)
Nachtigall W 1974 *Insects in Flight—A Glimpse Behind the Scenes in Biophysical Research* (London: Allen and Unwin)
Najjar F M and Mittal R 2003 Simulations of complex flows and fluid-structure interaction problems on fixed Cartesian grids *Proc. of FEDSM'03 4th ASME—JSME Joint Fluids Engineering Conf. FEDSM 2003-45577 (Honolulu, HI)*
Newman B G, Savage S B and Schouella D 1977 Model test on a wing section of a Aeschna dragonfly *Scale Effects in Animal Locomotion* ed T J Pedley (London: Academic) pp 445–77
Newman D J S and Wootton R J 1986 An approach to the mechanics of pleating in dragonfly wings *J. Exp. Biol.* **125** 361–72
Okamoto M, Yasuda K and Azuma A 1996 Aerodynamic characteristics of the wings and body of a dragonfly *J. Exp. Biol.* **199** 281–94
Piquet J and Vasseur X 2000 A nonstandard multigrid method with flexible multiple semi coarsening for the numerical solution of the pressure equation in a Navier–Stokes solver *Numer. Algorithms* **24** 333–55
Rees C J C 1975a Form and function in corrugated insect wings *Nature* **256** 200–3
Rees C J C 1975b Aerodynamic properties of an insect wing section and a smooth aerofoil compared *Nature* **258** 141–2
Rudolph R 1977 Aerodynamic properties of Libellula quadrimaculata L. (Anisoptera: Libelludidea), and the flow around smooth and corrugated wing section models during gliding flight *Odonatologica* **7** 49–58
Rüppell G 1989 Kinematic analysis of symmetrical flight maneuvers of odonata *J. Exp. Biol.* **144** 13–42
Savage S B, Newman B G and Wong D T M 1979 The role of vortices and unsteady effects during the hovering flight of dragonflies *J. Exp. Biol.* **83** 59–77
Schaffer S 1998 A semi coarsening multigrid method for elliptic partial differential equations with highly discontinuous and anisotropic coefficients *SIAM J. Sci. Comput.* **20** 228–42
Somps C and Luttges M 1985 Dragonfly flight: novel uses of unsteady separated flow *Science* **228** 1326–9
Sudo S and Tsuyuki K 2000 Wing morphology of some insects *JSME Int. J.* C **43** 895–900
Sun M and Lan L 2004 A computational study of the aerodynamic forces and power requirements of dragonfly (*Aeschna juncea*) hovering *J. Exp. Biol.* **207** 1897–901
Sunada S, Sakaguchi A and Kawachi K 1997 Airfoil section characteristics at low Reynolds number *J. Fluids Eng.* **119** 129–35
Thomas A L R, Taylor G K, Srygley R B, Nudds R L and Bomphrey R J 2004 Dragonfly flight: free-flight and tethered flow visualization reveal a diverse array of unsteady lift-generation mechanisms, controlled primarily via angle of attack *J. Exp. Biol.* **207** 4299–323
Udaykumar H S, Mittal R, Rampunggoon P and Khanna A 2001 A sharp interface Cartesian grid method for simulating flows with complex moving boundaries *J. Comput. Phys.* **174** 345–80
Vargas A 2006 Numerical investigation of the aerodynamic characteristics of a dragonfly wing section *PhD Dissertation* The George Washington University
Vogel S 1957 Flight in drosophila: III. Aerodynamic characteristics of fly wing and wing models *J. Exp. Biol.* **46** 431–43
Wakeling J M 1997 Odonatan wing and body morphologies *Odonatologica* **26** 35–52
Wakeling J M and Ellington C P 1997a Dragonfly flight: I. Gliding flight and steady-state aerodynamic forces *J. Exp. Biol.* **200** 543–56
Wakeling J M and Ellington C P 1997b Dragonfly flight: II. Velocity, acceleration, and kinematics of flapping flight *J. Exp. Biol.* **200** 557–82
Wang Z J 2000 Two dimensional mechanism for insect hovering *Phys. Rev. Lett.* **85** 2216–19
Wootton R J 1981 Support and deformability in insect wings *J. Zool.* **193** 447–68
Wootton R J 1990 The mechanical design of insect wings *Sci. Am.* **263** 114–20
Wootton R J 1991 The functional morphology of the insect wings of Odonata *Adv. Odonatol.* **5** 153–69
Wootton R J 1992 Functional morphology of insect wings *Annu. Rev. Entomol.* **37** 113–40
Wootton R J and Kukalová-Peck J 2000 Flight adaptations in Palaeozoic *Palaeoptera* (Insecta) *Biol. Rev.* **75** 129–67
Ye T, Mittal R, Udaykumar H S and Shyy W 1999 An accurate Cartesian grid method for viscous incompressible flows with complex immersed boundaries *J. Comput. Phys.* **156** 209–40